https://doi.org/10.1016/j.ymssp.2019.01.020

Structural damage detections based on a general vibration model identification approach

Chao Zhang[1, 2], Li Cheng[2, 3*], Jinhao Qiu[1*], Hongli Ji[1] and Jiayan Ji[1]

[1] State Key Laboratory of Mechanics and Control of Mechanical Structures, Nanjing University of Aeronautics and Astronautics, Nanjing, China

[2] Department of Mechanical Engineering, Hong Kong Polytechnic University, Hong Kong, China

[3] Hong Kong Branch of National Rail Transit Electrification and Automation Engineering Technology Research Center, Hong Kong Polytechnic University, Hong Kong, China

Submitted to *Mechanical Systems and Signal Processing*

Abstract

This paper presents a novel vibration-based damage detection method using a general vibration model identification (GVMI) approach. A damage index based on the identified general vibration model is constructed for damage detection and localization, with the damage

* Corresponding authors.

E-mail address: li.cheng@polyu.edu.hk (Prof. Li CHENG), qiu@nuaa.edu.cn (Prof. Jinhao QIU).

being regarded as a virtual excitation on the structure. The proposed GVMI approach utilizes a general form of high order derivative equation that to be identified and further used to detect changes in the vibration characteristics of the structure. Therefore, the proposed damage detection method requires neither baseline signals nor prior knowledge on the structural parameters, thus offering great application potentials for complex structures with unknown parameters. As a proof-of-concept example, a honeycomb sandwich cantilever beam is investigated for validating the proposed approach. The influences of the key parameters on the detection resolution, such as the measurement interval, the order of the displacement derivative and the selection of the excitation frequency, are investigated. Furthermore, an enhanced version of the GVMI method with an excitation frequency extension is developed by using a data fusion scheme. Taking advantages of the broadband excitations, the blind inspection area can be completely eliminated, whilst improving the effectiveness and the accuracy of the detection. Experimental results with both single and multiple structural damage show the validity and the accuracy of the proposed approach.

Keywords: Structural Vibration, Damage Detection, Data Fusion, Parameter Identification.

1. Introduction

Structural safety and integrity cannot be over-emphasized because the catastrophic structural failure may bring a great loss of human lives and wealth. Therefore, the demand for effective and reliable damage detection methods is ever-increasing during the recent decades. Many damage detection methods, such as ultrasonic [1, 2], radiography [3, 4], eddy current [5, 6], guided wave [7, 8], thermography [9, 10] *etc.* have been developed to detect and identify structural damage for various applications. Among them, vibration based methods have aroused the interest of many researchers [11-14]. Typically, various damage indices were constructed based on different vibration parameters such as stiffness, mode shape, natural frequency, electro-mechanical impedance or damping property to detect local structural damage [15-18]. The implementation of these methods calls for the use of different measurement equipment such as Laser Doppler Vibrometer (LDV), acceleration sensors, strain gauges and piezoelectric sensors [19-21].

However, the implementation of most vibration based methods has been somewhat hampered by their serious reliance on the global vibration models, boundary conditions, baseline signals *etc*. When the structural parameters in the healthy situation are inaccessible or the structure under inspection is too complex to be modelled, the detection is difficult to be achieved under practical circumstances. Most critically, such global-vibration based methods are insensitive to the local damage before it reaches a conspicuous level. In an earlier attempt to tackle these problems, the “pseudo-excitation” (PE) approach was developed to identify the occurrence of the damage by evaluating the local vibration characteristics of the structure [22-

25]. Since the inspection philosophy is local component specific, PE approach can be applied to a complex system by examining the corresponding local equation of motion component-by-component [26]. However, this approach still cannot solve the above problems completely, due to the inevitable requirement for the structural local equation of motion, especially given the discrepancies between the ideal and actual structural properties.

To address these problems, a novel damage detection method based on a general vibration model identification (GVMI) procedure is proposed in this paper. Different from the methods that directly use the theoretical and numerical vibration models, the proposed GVM approach assumes a general equation form, involving a series of high-order displacement derivatives and unknown physical parameters to approximate the dynamic characteristics of the structure under inspection. Combined with the least mean square (LMS) algorithm, the proposed method has great potential to be applied to complex structures with unknown parameters. Furthermore, a data fusion scheme with broadband frequency excitation is used instead of single frequency excitation, by which the enhanced damage index is shown to produce better detection results with significantly improved damage resolution.

This paper is organized as follows: in Section 2, the basic principle of the damage detection method based on GVMI is proposed, along with the detailed implementation procedure. In Section 3, numerical validations are presented using an aluminum honeycomb sandwich beam as an example. The selections of the optimized parameters such as the highest order of the displacement derivative, the measurement interval and the excitation frequency are investigated.

As a further improvement, an enhanced GVMI version using excitation frequency extension is developed, by which the blind area of the inspection is eliminated. Experiments are subsequently carried out to validate the proposed method. Finally, the conclusions are drawn.

2. Theory of the GVMI based damage detection

A practical engineering structure usually comprises various sub-structural components. With different compositions and boundary conditions, a description of the global dynamic properties such as mode shapes, natural frequencies and transient responses, maybe cumbersome or even impractical. However, within a specific local area, each structural component should satisfy a certain equation of motion, which can generally be described as

$$[\mathbf{F}_{int.}]+[\mathbf{F}_{iner.}]+[\mathbf{F}_{ext.}]=0 \tag{1}$$

where $[\mathbf{F}_{int.}]$ is the internal force induced by the structural deformation, $[\mathbf{F}_{iner.}]$ represents the inertia force related with the structural vibration and $[\mathbf{F}_{ext.}]$ is external excitation applied on the corresponding area. In the case of a pristine component in the absence of any external excitation, Eq. (1) becomes

$$[\mathbf{F}_{int.}]+[\mathbf{F}_{iner.}]=0 \tag{2}$$

in which $[\mathbf{F}_{int.}]$ can be written in a general form as

$$[\mathbf{F}_{int.}]=\left[\mathbf{L}\right]\cdot\left[\mathbf{u}\right] \tag{3}$$

where $[\mathbf{L}]$ is a matrix of spatial differential operator, $[\mathbf{u}]$ represents the structural vibration displacement vector.

Taking a one-dimensional structural component (a beam-like structure) under a flexural

harmonic excitation as an example, the steady transverse displacement $u(x)$ satisfies the general vibration model (GVM) mentioned in Eq. (2) as

$$\sum_i a_i u^{(i)}(x) = 0 \qquad (i = 0, 2, 4...) \tag{4}$$

where the superscript (i) denotes the order of the displacement derivative, a_i regroups various parameters of the structural geometry and material. The first term, a_0, can be written as

$$a_0 = -\rho S \omega^2 \tag{5}$$

where ρ and S are the density and cross area of the structure, and ω is the angular frequency. $a_0 u(x)$ represents the inertia force. However, with the occurrence of structural damage, changes in a_i are anticipated [23]. Thus, when pluging $u(x)$ within the damaged area into the equation with a_i taken in the healthy region, Eq. (4) should be different from zero. The residual quantity corresponds to a virtual excitation induced by the structural damage. Therefore, to identify the damage location in the structure, a damage index $DI(x)$ can be defined as the virtual external excitation according to the GVM, given by

$$DI(x) = \sum_i a_i u^{(i)}(x) \qquad (i = 0, 2, 4...) \tag{6}$$

The basic principle of the proposed method is based on an examination of the $DI(x)$ curve along the structure. The damage location can be detected wherever unexpected peaks appear in the $DI(x)$ curve. For a typical Euler-Bernoulli beam structure with homogeneous isotropic material properties, $DI(x)$ can be simplified as

$$DI(x) = a_4 u^{(4)}(x) + a_0 u(x) \tag{7}$$

where a_4 is flexural rigidity EI, in which E and I are the modulus of elasticity and the cross-sectional moment of inertia of the beam, respectively. a_0 is the product of the linear density of

the beam and vibration frequency as Eq. (5). However, Eq. (7) can be regarded as a special case of Eq. (6) and it is not applicable for a more complex structure, in which the theory of Euler-Bernoulli beam does not hold. It is worthy noting that the proposed method is, in principle, applicable anywhere inside the free surfaces and between structural supports. However, $DI(x)$ is naturally different from zero at the constraint positions and loading points. In principle, for points close to the supports or excitation points, this can always be done by reducing the measurement interval, but never exactly at these points.

The displacement of the beam structure under a steady vibration excitation can be usually measured point-by-point through a Laser Doppler Vibrometer (LDV). It converts the continuous displacement $u(x)$ into a series of discrete displacement values u_j, where the subscript j represents the j-th measurement point. The displacement derivative can be calculated by mean of the finite difference [23], as

$$u_j^{(i)} = \frac{\sum_{k=0}^{i} (-1)^k C_i^k u_{j+k-p}}{d^i} \qquad (i = 2p) \tag{8}$$

where C_i^k is the combination number and d is the interval between each pair of adjacent measurement points. Eq. (6) in the discrete form writes as:

$$\begin{bmatrix} DI_1 \\ DI_2 \\ \vdots \\ DI_N \end{bmatrix} = \begin{bmatrix} u_1 & u_1^{(2)} & \cdots & u_1^{(n)} \\ u_2 & u_2^{(2)} & \cdots & u_2^{(n)} \\ \vdots & \vdots & \ddots & \vdots \\ u_N & u_N^{(2)} & \cdots & u_N^{(n)} \end{bmatrix} \times \begin{bmatrix} a_0 \\ a_2 \\ \vdots \\ a_n \end{bmatrix} \tag{9}$$

where N is the number of the measurement points and n is the highest order of the displacement derivative. It should be mentioned that the above equations, which contain no first order derivative of the displacement with respect to t, are derived from an undamped structural

vibration model. The light damping only takes significant effect on the vibration mainly in the vicinity of structural resonances. Thus, without loss of generality, the damping influence can be ignored when excitation frequency is away from any natural frequencies of the structure.

To implement the damage detection process, a GVMI approach is proposed to identify a_i in Eq. (9) before the construction of the DI_i for the damaged structure. Assuming that the structural damage only occupies a small area of the whole structure, most part of the structure satisfies Eq. (4) within the inspection region in the absence of any external excitation. The general idea is to generate a coefficient vector $[a_i]$ to minimize the Mean Square Error (MSE) of the calculated DI_i, written as:

$$MSE = \sum_{i=1}^{N} DI_i^2 \Big/ N \tag{10}$$

In this paper, the LMS algorithm [27, 28] is used in GVMI to identify the coefficient vector $[\hat{a}_i]$, which can be given as

$$\left[\hat{a}_i\right] = \arg\min\left(MSE\right) \tag{11}$$

To summarize, the GVMI based damage detection can be implemented by taking the following steps as shown by the flowchart in Fig. 1:

Step 1: Excite the structure to generate the steady vibration and measure the displacement u_i within the inspection region.

Step 2: Select the highest order of the displacement derivative in the GVM and calculate the matrix $[u_j^{(i)}]$ according to Eq. (8).

Step 3: The GVMI can be achieved by identifying the coefficient vector $[\hat{a}_i]$ using the LMS

algorithm.

Step 4: The damage index at each measurement point can then be constructed using Eq. (9) with the identified parameter $[\hat{a}_i]$ and the structural damage can be located where a drastic change is observed in the DI_i curve.

Step 5: In order to eliminate the structural damage induced influence on the GVMI, use the detection result by Step 4 as a reference and extract the $[u_j^{(i)}]$ in the pristine area. Repeat Steps 3 and 4 with the $[u_j^{(i)}]$ in the pristine area to improve the detection result.

It can be seen from the Eq. (9) that the GVMI based damage detection is to examine the local breakage of the identified equation of motion point-by-point. The appealing features of the proposed method can be highlighted as follows:

1. The DI_i is calculated from the vibration displacement curve of the structure in the current status. Thus, no benchmark structural models or baseline signals are needed *a priori*.
2. The DI_i is based on a local examination of the local dynamic property of the structure, independently of the rest of the system. Therefore, the proposed method requires no knowledge on factors such as the boundary conditions and the global structural model.
3. The GVM can be used to characterize the dynamics of more complex structural components. Considering a structure as a combination of basic structural components such as beams, plates and shells, the proposed damage detection methodology can be applied to each segment of the structure based on its local inspection nature. The applicability of the method is therefore not limited to simple homogeneous components.

4. In theory, as long as the structure is under steady vibration, the damage detection can be implemented. No additional requirements for the excitation source are needed.
5. Any structural damage that breaks the local dynamics of the structure can be detected, inrespective of the number of structural damage.

It is worthy noting that the GVMI based damage detection physlosophy is not limited to the beam-like structures only. Similarly, a two-dimensional damage index $DI_{i,j}$ can be derived for a plate-like structural components by using a high order partial derivative equation to approximate the GVM.

3. Numerical validations

3.1 Finite element model

Lightweight materials are especially attractive in the civil, aeronautical and aerospace industries. Among various types of lightweight materials, the honeycomb sandwich material is commonly seen, with high strength-to-weight ratio, enhanced bending stiffness and good damage tolerance [29, 30]. Thus, it is widely used in aircraft wings, antenna structures, bridges and so on. A proof-of-concept validation of the proposed GVMI based damage detection method is firstly carried out using Finite Element Method (FEM). Without loss of generality, a one-dimensional structure (an aluminum honeycomb sandwich beam) is taken as an example.

As shown in Fig. 2, the beam component under investigation consists of two continuous aluminum face sheets, which are separated by a layer of low-density core (aluminum

honeycomb). The thickness of the face sheet is 1 mm, while that of the honeycomb core is 5 mm. The honeycomb is made of 0.05 mm thick aluminum foil and the length of the honeycomb element is 6 mm. The whole beam structure is 685 mm long and 42 mm wide. A simplified FE model as shown in Fig. 2 using 3D solid elements is created using commercial FE code ABAQUS. In order to accurately obtain the vibration displacement on the surface with the equal spacing measurement points, the face sheet is divided into several uniform squares with a length of 1 mm in plane, resulting in a total of 28770 elements in each face sheet. A harmonic point-excitation is applied at x = 676 mm (the coordinate system is shown in Fig. 2 and the coordinate origin starts from the left point of the inspection region). The excitation frequency f is set to 700 Hz. Two different types of structural damage are investigated in this paper. The first one is a surface slit extending uniformly along the width of the beam placed on the face sheet. The slit is 2 mm wide and penetrates the face sheet in thickness. The second one is a simulated delamination containing a slit placed in the honeycomb core under the face sheet with 2 mm in width and 2 mm in thickness. The center of the structural damage is located at $x=l_d$, which is 297 mm in both cases. Fig. 3 shows the flexural displacement w_i at each element node with a slit on the face sheet. Considering that the basic principle of the proposed method is independent of the excitation level and the amplitude of the excitation can be arbitrary, w_i is shown in form of the normalized displacement. To validate the noise immunity capability of the proposed method, a random Gaussian white noise with a standard deviation of 1% in amplitude, corresponding to 40 dB of the signal-to-noise ratio (SNR) in energy, is added to the simulated displacement.

3.2 Results and discussions

The accuracy of the GVM is governed by the highest order of the displacement derivative n in Eq. (9). n=4 is firstly used to model the structure in the numerical validation. With the noisy displacement w_i in Fig. 3, the normalized DI_i curves constructed through Step 1 to Step 5 is shown in Fig. 4. Considering that the accuracy of the finite difference used in the calculation of the displacement derivatives $[u_j^{(i)}]$ is related to the measurement interval d, a small d is, in principle, required to achieve a high accuracy of the finite difference and to improve the resolution of damage detection. However, it leads to dense measurement points and increases the sensitivity of the DI_i to the measurement noise. To explore this issue, five different intervals are selected and compared in Fig. 4, using 1 mm, 4 mm, 8 mm, 10 mm and 12 mm, respectively. For a quantitative comparison of the detection results, a *DI*-to-noise ratio, *DINR*, is defined as:

$$DINR = \frac{\overline{DI}_d}{\overline{DI}_h} \tag{12}$$

where $\overline{DI}_d$ and $\overline{DI}_h$ are the average values of the damage index in the damage area and healthy area, respectively. It is apparent that *DINR* is a measure to evaluate the level of a desired detection result compared with the background noise and a higher *DINR* indicates a better detection resolution. As listed in Table 1, when d increases, *DINR* is significantly improved when d is below 8 mm and reaches the maximum when d=10 mm, in agreement with previous observations made using a model-based homogeneous beam strcutures [23]. Therefore, d=10 mm is used as the optimal measurement interval in the following discussions. It should be mentioned that other signal de-nosing techniques, such as wavelet transform, low-pass wavenumber filtering and "weak" form of damage detection [22-26], could also be used as additional means to enhance the robustness of the proposed damage detection strategy under

noisy measurement conditions. In this paper, the adjustment of the measurement density is opted as the simplest way to improve the *DINR*. The main advantage is that no additional signal processing method is required. However, as the measurement interval increases, the resolution of the detection decreases as well.

Detection results using n=4 and n=6 are shown in Fig. 5. It can be seen that both allow the damage identifications with a high resolution. Altghough n=6 can achieve a more precise characterization of the structural vibration, DI_i will be more sensitive to the measurement noise as the derivative order in finite difference increases. Therefore, in the present case, n=4 seems to be sufficient for the damage detection. The detection results also indirectly prove that the identified GVM can reflect the vibration characteristics of the objective. However, it should be mentioned that this GVM is only valid when the cantilever beam is excitied at f=700 Hz. Considering the structural complexity, it is difficult to use a particular GVM to model the vibration characteristics of the honeycomb stucutre at arbitrary frequency.

Delamination is another typical type of damage in the honeycomb sandwich beam. Since the proposed method interrogates whether the measured vibration displacement satisfies the local dynamics under the healthy condition, in principle, any changes in the structure can be detected. Having said that, it is understandable that the detection accuracy of the proposed approach may deteriates or even fails when the structural damage is too small to alter the local dynamics of the struture distinctly. For the simulated delamination case shown in Fig. 2, the flexural displacement at each element node is calculated, when the excitation frequency is set

to 700 Hz as shown in Fig. 6. The noise, of the same level as the case in Fig.3, is added to the displacement. Detection result using d=10 mm and n=4 is shown in Fig. 7, which shows that the proposed method can successfully detect the structural damage with different types and sizes.

To further test and verify the proposed method, ten cases (from case 1 to 10) with different slit locations are comparatively used to construct DI_i in the simulation. Fig. 8 shows the vibration displacement of the discussed beam without slit and the locations of the structural damage in each case. The slits in case 1 and case 10 are respectively located near the peak (Point A at x=335 mm) and the node (Point B at x=380 mm) of the vibration displacement. Other cases involve slits which are eaqualy distributed within this quarter of the displacement wavelength. It should be mentioned that the displacement used to construct the DI_i in all cases are added with a Gaussian white noise of 40 dB in SNR. As shown in Fig. 9, whilst approaching Point B, the constructed DI_i gradually loses its capacity of identifying the structural damage location from case 1 to case 10, with the damage near the node of the vibration displacement. To quantify this effect, a normalized distance X_n between the damage location and the closest displacement node is defined as

$$X_n = \frac{|l_n - l_d|}{\lambda/4} \tag{13}$$

where l_d and l_n is the positions of the damage and the closest displacement node, λ is the wavelength of the vibration displacement. The variation of the *DINR*s against X_n in these ten cases are illustrated in Fig. 10. It shows that the resolution of the damage detection is dependent on X_n and the damage can hardly be detected when X_n is below 0.5, called blind area.

3.3 Enhanced GVMI using excitation frequency extension

Aimed at circumventing this problem, an enhanced GVMI method is proposed through enriching the excitation frequency content. Allowing for the fact that the wavenumber of the vibration displacement (consequently the location of the nodes) depends on the excitation frequency f, the position of the vibration node can be shifted through a judicious selection of f. For a better illustration, the displacement distributions with different excitation frequencies (f_l=600 Hz and f_h=800 Hz) in case 1 are shown in Fig. 11(a) and (b). Corresponding to these two frequencies, the displacement wavelengthes are, respectively, 281 mm and 235 mm. The vibration node in the vicinity of the damage shifts more than 50 mm, exceeding the length of the blind area. Therefore, the blind areas at f_l and f_h are not overlapped, making it possible to provide a comprehensive detection without any blind area with excitation frequency extension.

Reaching this stage, the constructed DI_i can be obtained under different excitation frequencies, denoted by $DI_{i\text{-}f}$. A data fusion scheme can subsequently be implemented to construct an enhanced damage index EDI_i, which is the maximum of the normalized damage index $NDI_{i\text{-}f}$ within the excitation frequency range, given as

$$EDI_i = \max\left(NDI_{i-f}\right) \tag{14}$$

where

$$NDI_{i-f} = \frac{DI_{i-f}}{\sum_{j=1}^{N} DI_{j-f}} \tag{15}$$

This data fusion scheme can generally be regarded as a statistical process for aggregating the results obtained under different excitation circumstances. EDI_i is an ultimate damage index,

defined within an excitation frequency range and applied to each measurement point i, which aims at improving the damage localization resolution and eliminating the blind area of the detection.

For illustration purposes, the ten cases shown in Fig. 8 are used again to validate the proposed method. Fig. 12 shows the distribution of $NDI_{i\text{-}f}$ in each case. The excitation frequency ranges from 600 Hz to 800 Hz. The resolution of the swept-frequency measurement is 10 Hz. In fact, Fig. 9 can be regarded as a special case of Fig. 12, that is only captured at f=700 Hz. However, the structural damage in case 5 to 10, which cannot be detected using Fig. 9, is identified with other excitation frequency in Fig. 12. It proves that the excitation frequency extension can eliminate the blind area effectively. The constructed EDI_i using Eq. (14) is presented in Fig. 13, in which the damage position can be clearly identified. Furthermore, to make a quantitative comparison, $DINR$s of each case using EDI_i are added to Fig. 10 to compare with the results using single excitation frequency. It is obvious that the enhanced GVMI method using EDI_i allows the detection of structural damage in all cases, thus eliminating the blind area observed before.

4. Experimental validations

4.1 Experimental setup

A honeycomb sandwich cantilever beam, made of aluminum 6061, is subsequently tested for the experimental validation. The honeycomb sandwich is 8 mm in thickness, covered by two face sheets on each side of 1 mm thick. The detailed dimensions of the entire beam structure

are shown in Fig. 14 and the material properties are listed in Table 2. The artificial structural damage is a rectangular slit, which is 2 mm in width penetrating the face sheet in thickness as illustrated in Fig. 14. During the experiments, both single structural damage (damage 1) and dual structural damage (damage 1 and 2) cases are tested. The beam is fix-supported on a testing table and excited by an electro-mechanical shaker. Through a power amplifier, the shaker provides a harmonic point-excitation to the structure at x=620 mm (referring to the coordinate system in Fig. 14 and the coordinate origin is located at the left point of the inspection region). As explained in Section 3, the excitation frequency range is set from 600 Hz to 800 Hz with a swept-frequency resolution equal to 10 Hz. A scanning Laser Doppler Vibrometer is used to measure the out-of-plane vibration displacement on the face sheet. Note that the measurement is conducted on the intact face sheet of the beam to avoid any influence of the slit on the displacement measurement. The interval between two adjacent measurement points is set to 1.8 mm.

4.2 Results and discussions

With a single slit located at x=410 mm, Fig. 15 shows the steady-state vibration displacement w_i, measured by the LDV at f=700 Hz. The structural damage is close to the displacement peak, facilitating the detection by GVMI based damage index DI_i. The constructed DI_i curve across the inspection range using Eq. (9) is presented in Fig. 16(a), in which the damage can be roughly identified with a measurement interval d_1=1.8 mm. However, measurement noise induced peaks in the DI_i curve may lead to possible misjudgments in the result. Treated with d_2=9.1 mm (d_2=5d_1), the DI_i curve is shown in Fig. 16(b), in which the

damage position is highlighted prominently. Conclusively, by reducing the number of the measurement points from 320 to 64, the influence of the measurement noise on the DI_i curve is significantly reduced. The *DINR* shown in Figs. 16 (a) and (b) is improved from 1.6 to 6.9, emphasizing an improved noise immunity capability with a proper selection of the measurement interval, in agreement with the numerical analyses reported in the previous sections.

The dual structural damage case is also tested in the experiment. Two slits are located at x=90 mm and x=410 mm, respectively. The proposed enhanced GVMI using enriched excitation frequency is carried out within a swept frequency range from 600 Hz to 800 Hz. According to Eq. (15), the constructed $NDI_{i\text{-}f}$ is ploted in Fig. 17. Since X_n of each structural damage varies with the the excitation frequency, the two slits have their respective blind frequency areas, in which the damage induced peak in $NDI_{i\text{-}f}$ is not pronounced. For example, with 720 Hz (Fig. 18), the slit at x=90 mm cannot be delineated (the corresponding X_n is below to 0.5). Thanks to the data fusion scheme in Eq. (14), both slits are clearly identified in Fig. 19 with the enhenced EDI_i curve.

5. Conclusions

A novel damage detection method, based on a general vibration model identification (GVMI) approach, is developed in this paper. Compared with the methods based on the theoretical vibration models, the proposed method constructs a damage index using an identified General Vibration Model (GVM), involving a series of high-order displacement

derivatives and unknown physical parameters to approximate the dynamic characteristics of the structure under inspection. For this reason, this method can be implemented for complex structural system with unknown parameters. Taking a honeycomb sandwich cantilever beam for verifications, both the simulations (added with a 40 dB Gaussian white noise in displacement) and the experiments are carried out to detect the structural damage positions. The influences of the key parameters on the detection resolution, such as measurement interval d, the highest order of the displacement derivative n, and the selection of the excitation frequency f, are investigated. For this study, the optimal d and n are 10 mm and 4, respectively. Detection results also indicate that the blind area exists when the detection is implemented using single excitation frequency. The structural damage can hardly be detected when X_n is below 0.5. An enhanced GVMI using excitation frequency extension (from 600 Hz to 800 Hz) is then proposed in this study to eliminate the blind area. Finally, both single and dual structural damage detection results show its validity and accuracy.

Acknowledgments

This work was supported partially by China Postdoctoral Science Foundation funded project (2017M621741), Jiangsu Planned Projects for Postdoctoral Research Funds (1701103C), Aeronautical Science Fund (20161552014 and 20170252005), Natural Science Foundation of Jiangsu Province (SBK2018040537) and National Natural Science Foundation of China (51775267 and 51805261). The corresponding author would like to thank the grant support from the Innovation and Technology Commission of the HKSAR Government to the Hong Kong Branch of National Rail Transit Electrification and Automation Engineering

Technology Research Center.

References

[1] B. W. Drinkwater, P. D. Wilcox, Ultrasonic arrays for non-destructive evaluation: A review, NDT & E International, 39 (2006) 525-541.

[2] S. Kolkoori, C. Hoehne, J. Prager, M. Rethmeier, M. Kreutzbruck, Quantitative evaluation of ultrasonic C-scan image in acoustically homogeneous and layered anisotropic materials using three dimensional ray tracing method, Ultrasonics, 54 (2014) 551-562.

[3] D. Bull, L. Helfen, I. Sinclair, S. Spearing, T. Baumbach, A comparison of multi-scale 3D X-ray tomographic inspection techniques for assessing carbon fibre composite impact damage, Composites Science and Technology, 75 (2013) 55-61.

[4] D. J. Bull, S. M. Spearing, I. Sinclair, L. Helfen, Three-dimensional assessment of low velocity impact damage in particle toughened composite laminates using micro-focus X-ray computed tomography and synchrotron radiation laminography, Composites Part A Applied Science & Manufacturing, 52 (2013) 62-69.

[5] J. Cheng, H. Ji, J. Qiu, T. Takagi, T. Uchimoto, N. Hu, Novel electromagnetic modeling approach of carbon fiber-reinforced polymer laminate for calculation of eddy currents and eddy current testing signals, Journal of Composite Materials, 49 (2014) 77-85.

[6] C. A. Stott, P. R. Underhill, V. K. Babbar, T. W. Krause, Pulsed eddy current detection of cracks in multilayer aluminum lap joints, Sensors Journal IEEE, 15 (2015) 956-962.

[7] Z. Su, C. Zhou, M. Hong, L. Cheng, Q. Wang, X. Qing, Acousto-ultrasonics-based fatigue damage characterization: Linear versus nonlinear signal features, Mechanical Systems & Signal

Processing, 45 (2014) 225-239.

[8] C. Zhang, J. Qiu, H. Ji, Laser ultrasonic imaging for impact damage visualization in composite structure, EWSHM-7th European Workshop on Structural Health Monitoring, Nantes, 01022980 (2014) 2199-2205.

[9] A. Maier, R. Schmidt, B. Oswald-Tranta, R. Schledjewski, Non-destructive thermography analysis of impact damage on large-scale CFRP automotive parts, Materials, 7 (2014) 413-429.

[10] P. Theodorakeas, N. P. Avdelidis, I. Hatziioannidis, E. Cheilakou, R. Marini, M. Koui, Comparative evaluation of aerospace composites using thermography and ultrasonic NDT techniques, Proceedings of SPIE - The International Society for Optical Engineering, 9485 (2015) 1-12.

[11] W. Fan, P. Qiao, Vibration-based damage identification methods: A review and comparative study, Structural Health Monitoring, 9 (2010) 83-111.

[12] Y. J. Yan, L. Cheng, Z. Y. Wu, L. H. Yam, Development in vibration-based structural damage detection technique, Mechanical Systems & Signal Processing, 21 (2007) 2198–2211.

[13] S. Das, P. Saha, S.K. Patro, Vibration-based damage detection techniques used for health monitoring of structures: a review, Journal of Civil Structural Health Monitoring, 6 (2016) 1-31.

[14] C. R. Farrar, K. Worden, An introduction to structural health monitoring, Philos Trans A Math Phys Eng Sci, 365 (2010) 303-315.

[15] M. Radzieński, M. Krawczuk, M. Palacz, Improvement of damage detection methods based on experimental modal parameters, Mechanical Systems & Signal Processing, 25 (2011) 2169-2190.

[16] S. Weng, H. P. Zhu, Y. Xia, L. Mao, Damage detection using the eigenparameter decomposition of substructural flexibility matrix, Mechanical Systems & Signal Processing, 34 (2013) 19-38.

[17] S. Na, H. K. Lee, A technique for improving the damage detection ability of the electro-mechanical impedance method on concrete structures, Smart Materials & Structures, 21 (2012) 85024-32.

[18] J. T. Kim, Y. S. Ryu, H. M. Cho, N. Stubbs, Damage identification in beam-type structures: frequency-based method vs mode-shape-based method, Engineering Structures, 25 (2003) 57-67.

[19] C. Zhang, L. Cheng, J. Qiu, H. Wang, Damage detection based on sparse virtual element boundary measurement using metal-core piezoelectric fiber, Structural Health Monitoring, 17 (2018) 15-23.

[20] U. Galvanetto, C. Surace, A. Tassotti, Structural damage detection based on proper orthogonal decomposition: experimental verification, AIAA Journal, 46 (2015) 1624-1630.

[21] H. Chen, M. Kurt, Y. S. Lee, D. M. Mcfarland, L. A. Bergman, A. F. Vakakis, Experimental system identification of the dynamics of a vibro-impact beam with a view towards structural health monitoring and damage detection, Mechanical Systems & Signal Processing, 46 (2014) 91-113.

[22] M. Cao, L. Cheng, Z. Su, H. Xu, A multi-scale pseudo-force model in wavelet domain for identification of damage in structural components, Mechanical Systems & Signal Processing, 28 (2012) 638–659.

[23] H. Xu, L. Cheng, Z. Su, J. L. Guyader, Identification of structural damage based on locally

perturbed dynamic equilibrium with an application to beam component, Journal of Sound & Vibration, 330 (2011) 5963–5981.

[24] H. Xu, L. Cheng, Z. Su, J. L. Guyader, Damage visualization based on local dynamic perturbation: Theory and application to characterization of multi-damage in a plane structure, Journal of Sound & Vibration, 332 (2013) 3438-3462.

[25] M. S. Cao, W. Ostachowicz, M. Radzienski, W. Xu, Multiscale shear-strain gradient for detecting delamination in composite laminates, Applied Physics Letters, 103 (2013) 101910-14.

[26] C. Zhang, L. Cheng, H. Xu, J. H. Qiu, Structural damage detection based on virtual element boundary measurement, Journal of Sound & Vibration, 372 (2016) 133-146.

[27] M. Nayyerloo, J. G. Chase, G. A. Macrae, X. Q. Chen, LMS-based approach to structural health monitoring of nonlinear hysteretic structures, Structural Health Monitoring, 9 (2010) 429-444.

[28] T. Wassereau, C. Pézerat, J. L. Guyader, F. Ablitzer, Characterization of materials and flaw detection using force analysis technique, Inter-noise and Noise-con Congress and Conference Proceedings, (2015) 452-462.

[29] K. Zhu, M. Chen, Q. Lu, B. Wang, D. Fang, Debonding detection of honeycomb sandwich structures using frequency response functions, Journal of Sound & Vibration, 333 (2014) 5299-5311.

[30] M. Yang, P. Qiao, Quasi-static indentation behavior of honeycomb sandwich materials and its application in impact simulations, Journal of Aerospace Engineering, 21 (2008) 226-234.

Table and Figure Captions

Tables

Table 1. *DINR*s of damage detections with different measurement intervals *d*.

d (mm)	1	4	8	10	12
DINR	0.74	2.28	4.01	5.24	5.10

Table 2. Structural parameters of the cantilever beam used in the experiment.

Beam width [mm]	40
Length of honeycomb element [mm]	6
Al foil used in honeycomb [mm]	0.05
Density [kg/m^3]	2700
Elastic modulus [GPa]	68.9

Figures

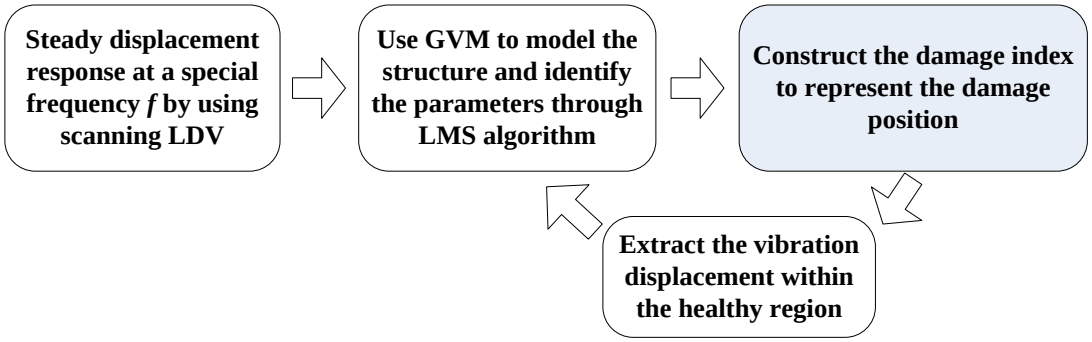

Fig. 1. Flow chart on the procedure of constructing damage index using GVMI.

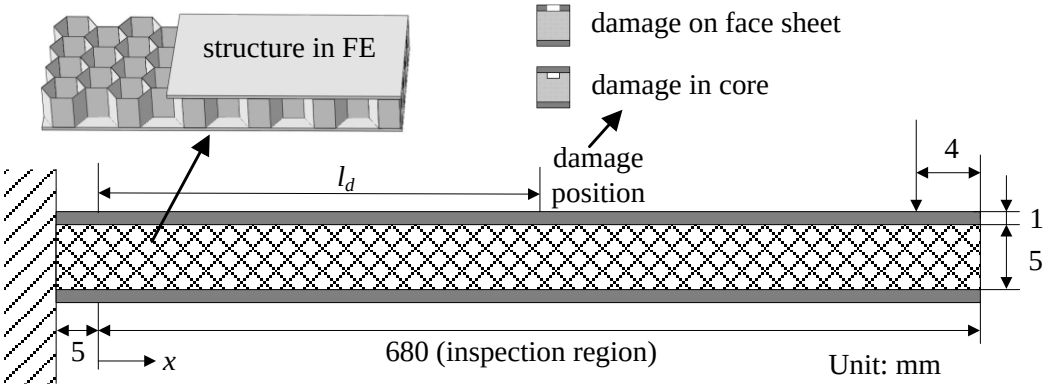

Fig. 2. A honeycomb sandwich beam with artificial damage used in simulation.

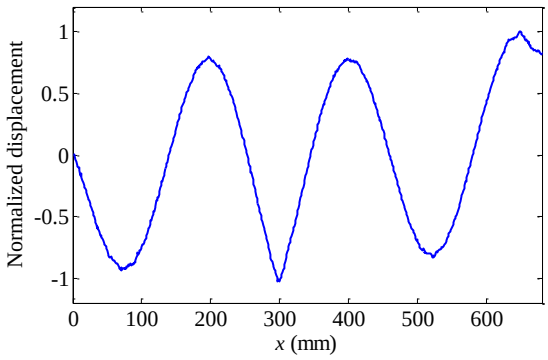

Fig. 3. Normalized displacement with noise with a slit on face sheet at x=297 mm.

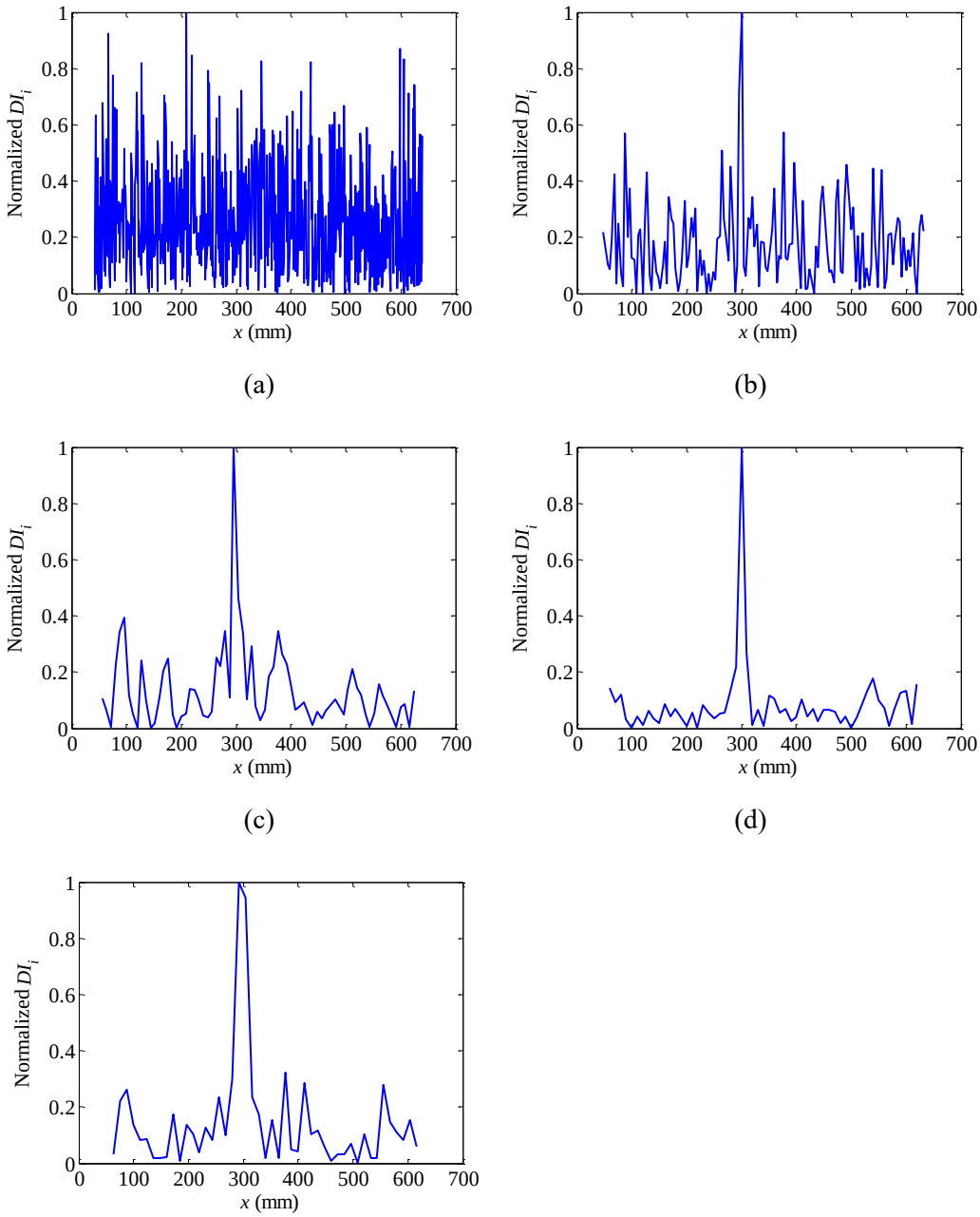

Fig. 4. Normalized DI_i with different measurement interval d:

(a) d=1 mm; (b) d=4 mm; (c) d=8 mm; (d) d=10 mm; (e) d=12 mm.

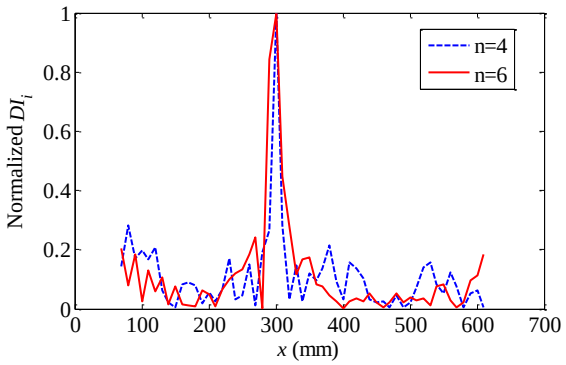

Fig. 5. Normalized DI_i with different highest order of displacement derivatives n.

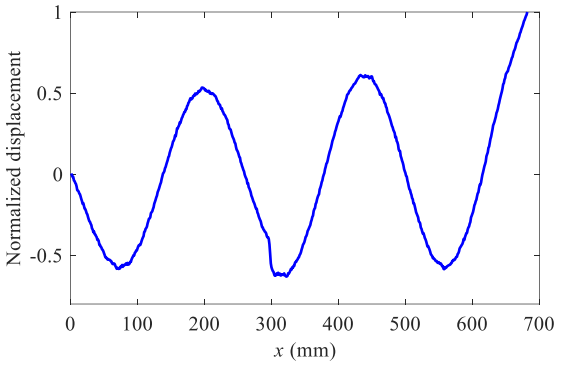

Fig. 6. Normalized displacement with noise with a delamination at x=297 mm.

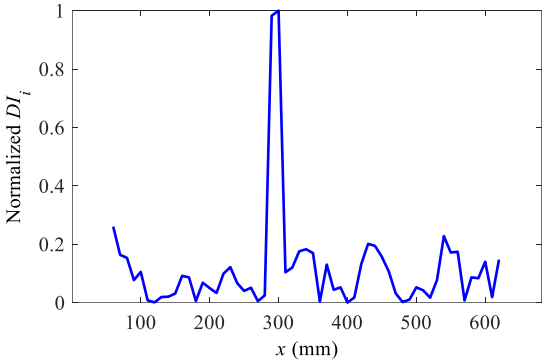

Fig. 7. Normalized DI_i calculated from the vibration displacement with a delamination.

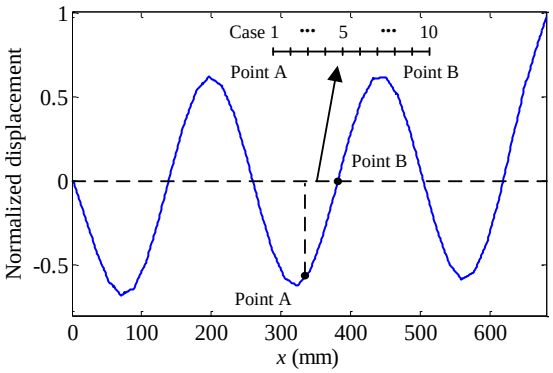

Fig. 8. Damage positions in ten cases against the structural displacement.

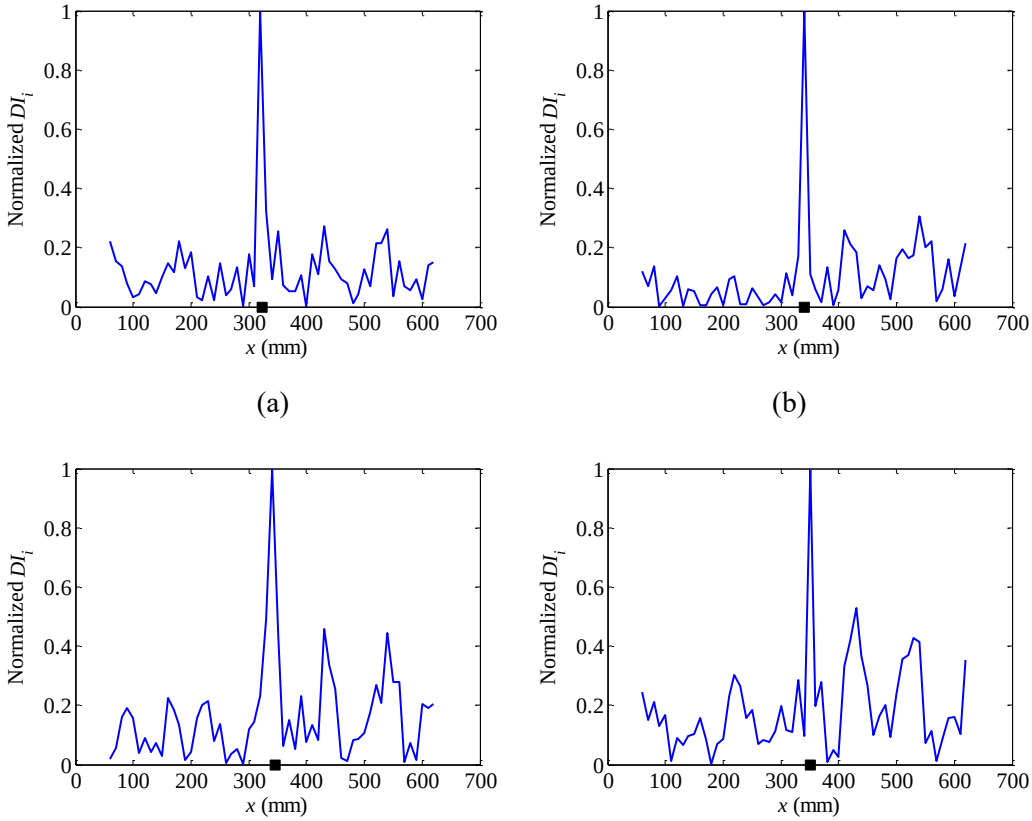

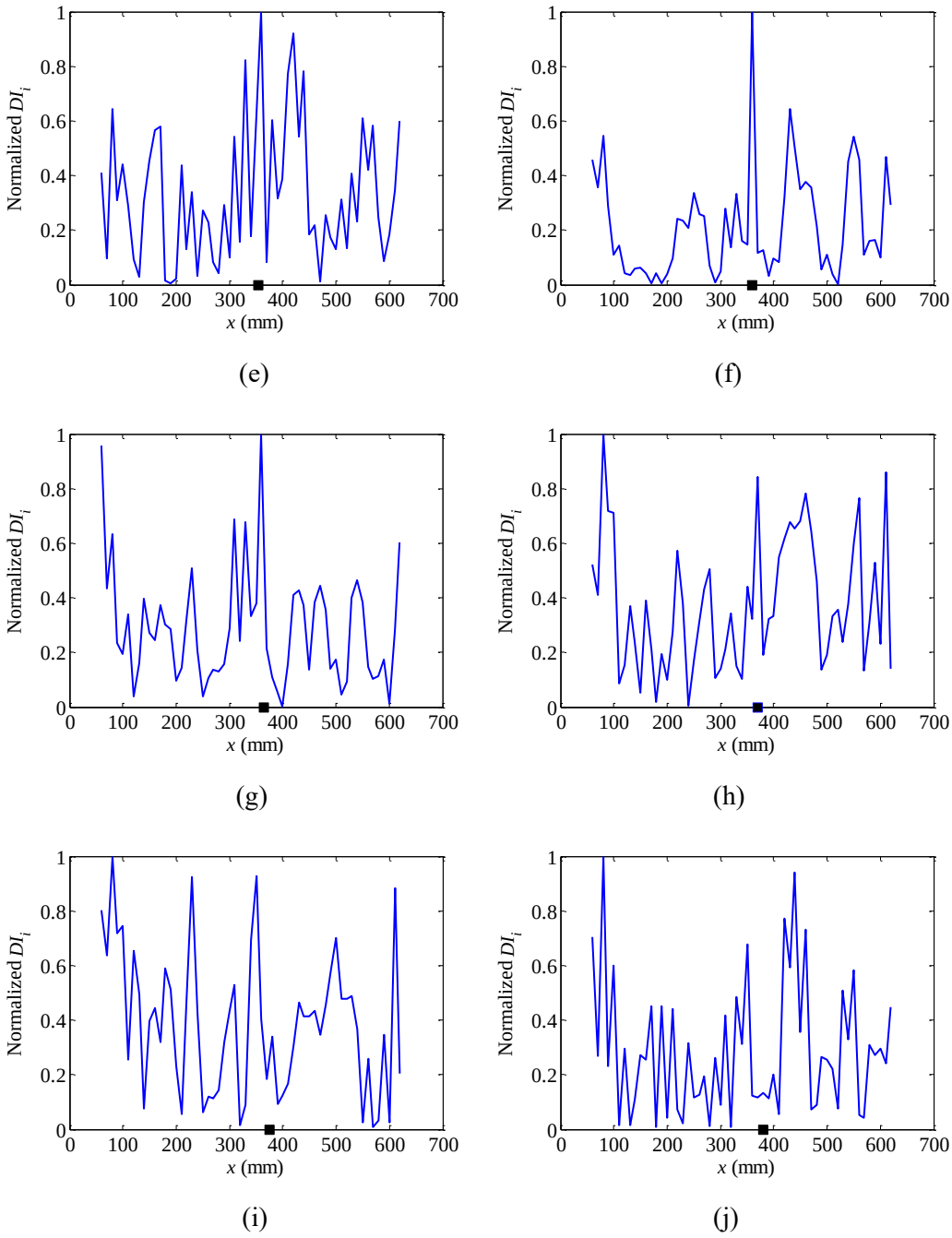

Fig. 9. Results using normalized DI_i with different X_n: (a)-(j) refer to case 1-10.

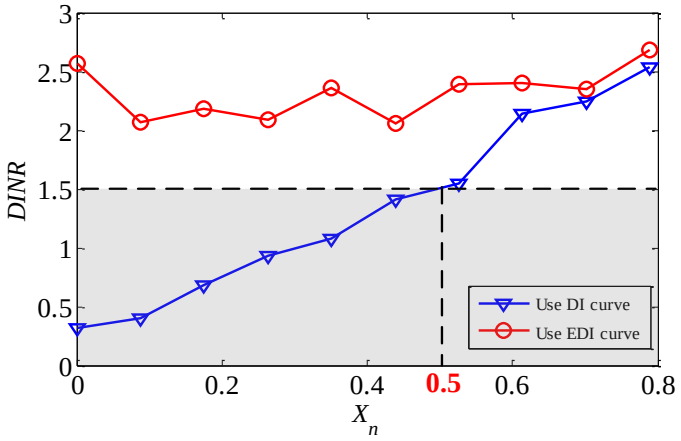

Fig. 10. The resolution of detection results *DINR*s against X_n.

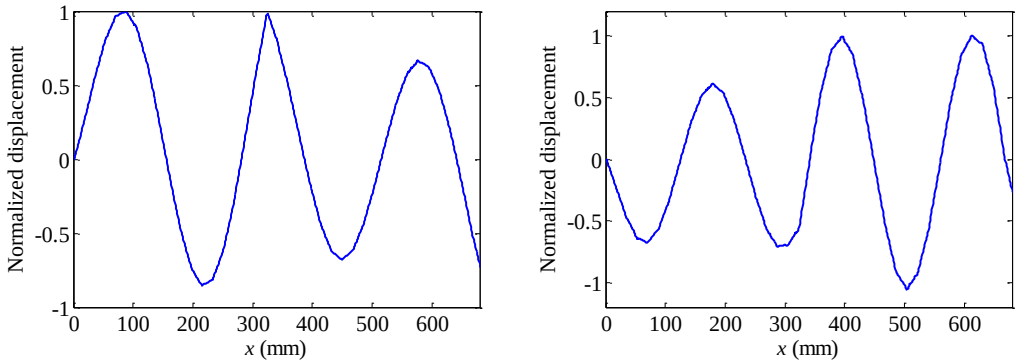

Fig. 11. Normalized displacements at different frequency: (a) f=600 Hz; (b) f=800 Hz.

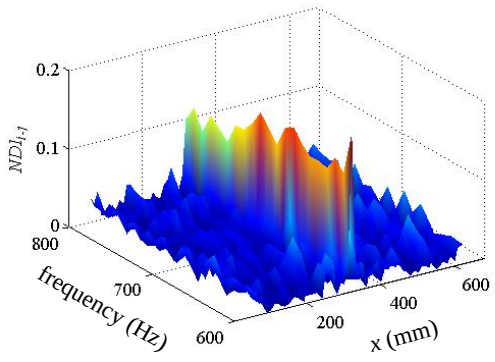
0.2
0.1
0
NDI_{i-1}
800
700
600
frequency (Hz)
200
400
600
x (mm)

(a)

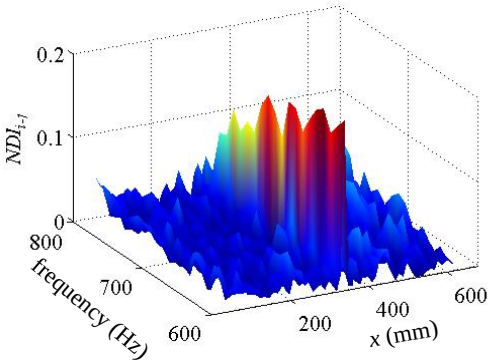
0.2
0.1
0
NDI_{i-1}
800
700
600
frequency (Hz)
200
400
600
x (mm)

(b)

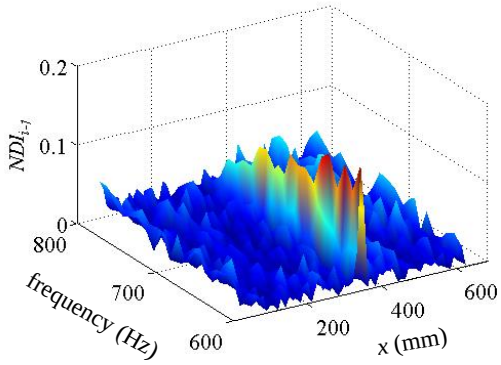
0.2
0.1
0
NDI_{i-1}
800
700
600
frequency (Hz)
200
400
600
x (mm)

(c)

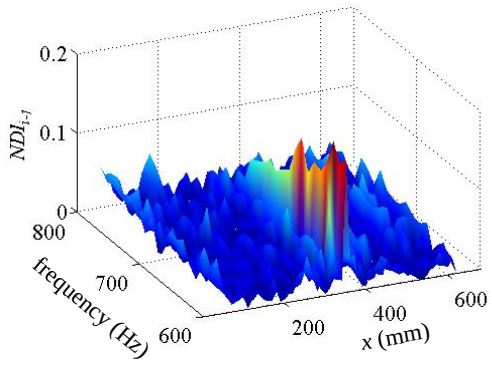
0.2
0.1
0
NDI_{i-1}
800
700
600
frequency (Hz)
200
400
600
x (mm)

(d)

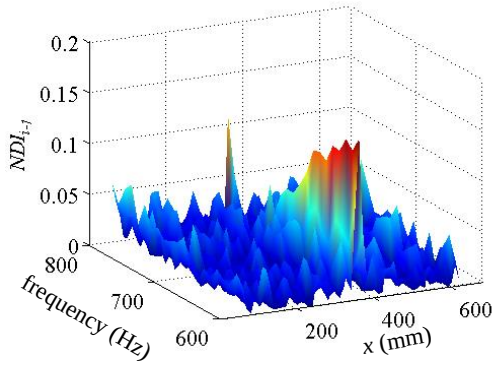
0.2
0.15
0.1
0.05
0
NDI_{i-1}
800
700
600
frequency (Hz)
200
400
600
x (mm)

(e)

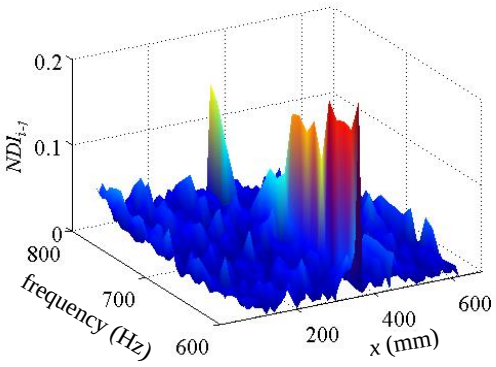
0.2
0.1
0
NDI_{i-1}
800
700
600
frequency (Hz)
200
400
600
x (mm)

(f)

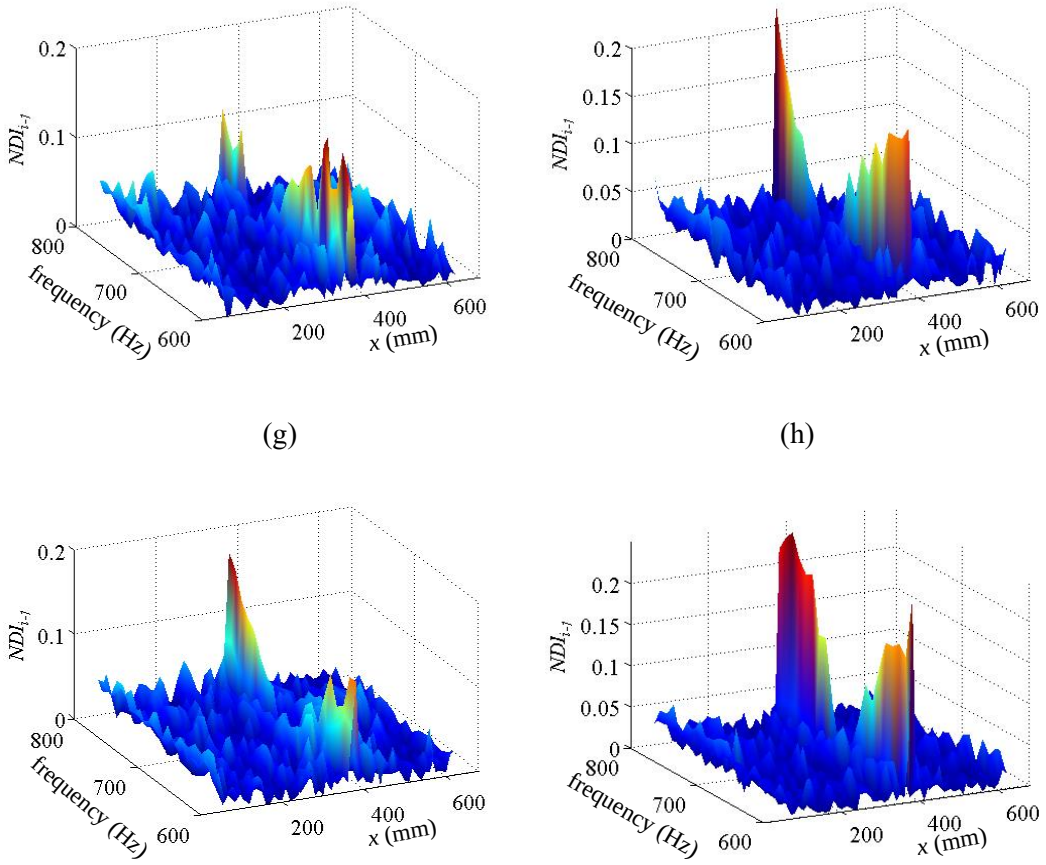

Fig. 12. Results using NDI_{i-f} with different X_n: (a)-(j) refer to case 1-10.

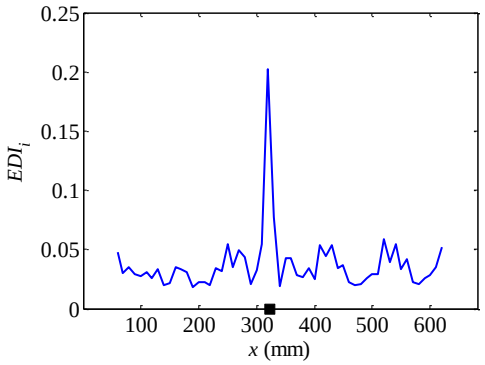
0.25
0.2
0.15
0.1
0.05
0
EDI_i
100 200 300 400 500 600
x (mm)

(a)

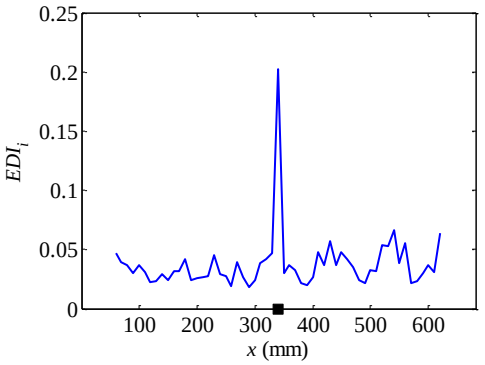
0.25
0.2
0.15
0.1
0.05
0
EDI_i
100 200 300 400 500 600
x (mm)

(b)

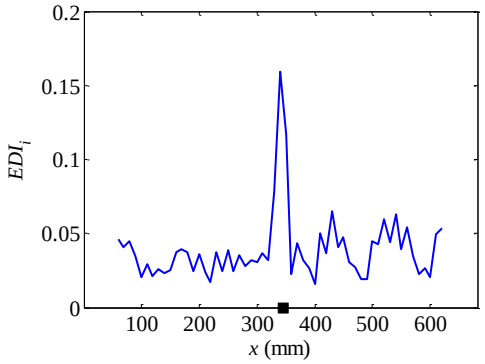
0.2
0.15
0.1
0.05
0
EDI_i
100 200 300 400 500 600
x (mm)

(c)

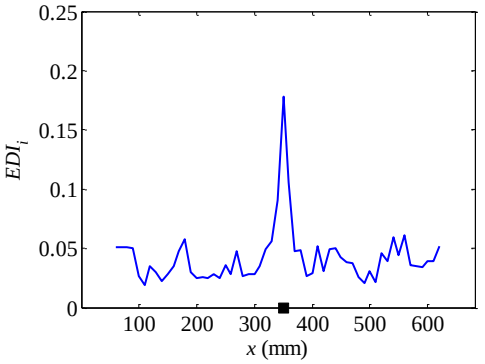
0.25
0.2
0.15
0.1
0.05
0
EDI_i
100 200 300 400 500 600
x (mm)

(d)

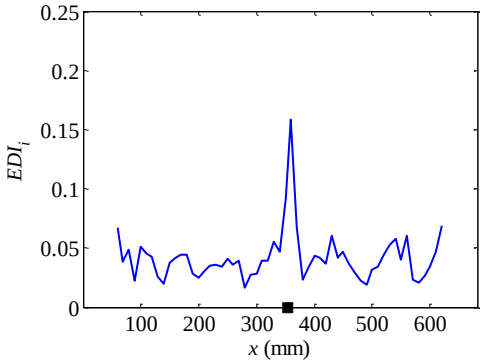
0.25
0.2
0.15
0.1
0.05
0
EDI_i
100 200 300 400 500 600
x (mm)

(e)

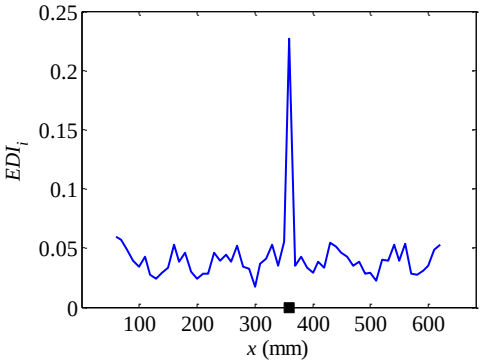
0.25
0.2
0.15
0.1
0.05
0
EDI_i
100 200 300 400 500 600
x (mm)

(f)

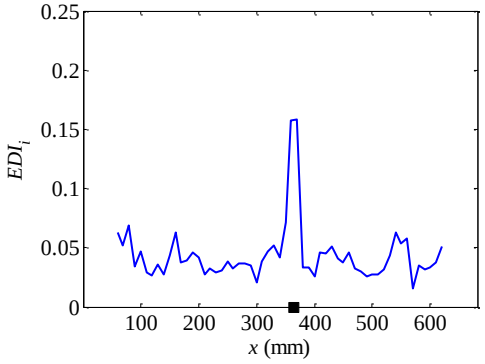
0.25
0.2
0.15
0.1
0.05
0
EDI_i
100 200 300 400 500 600
x (mm)

(g)

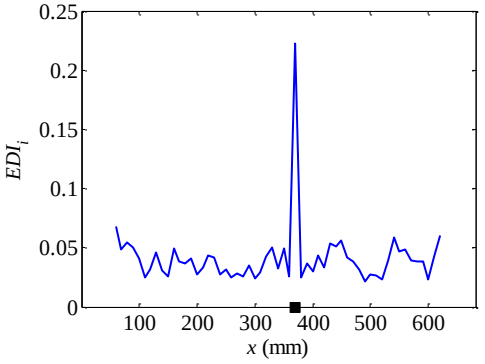
0.25
0.2
0.15
0.1
0.05
0
EDI_i
100 200 300 400 500 600
x (mm)

(h)

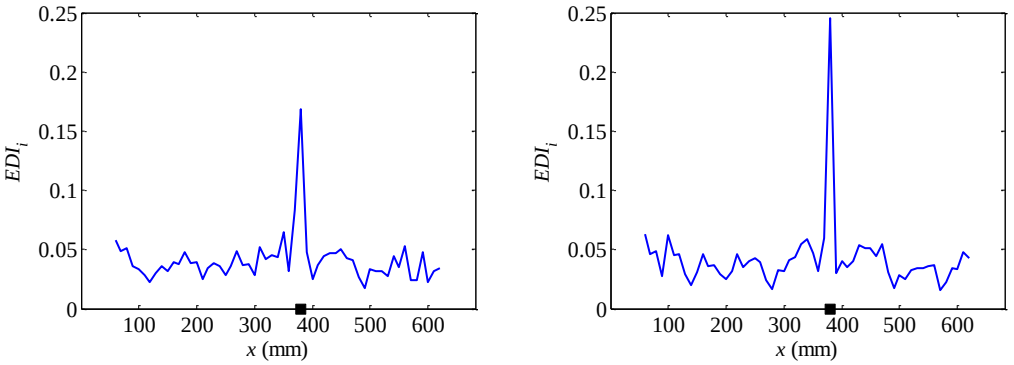

Fig. 13. Results using EDI_i with different X_n: (a)-(j) refer to case 1-10.

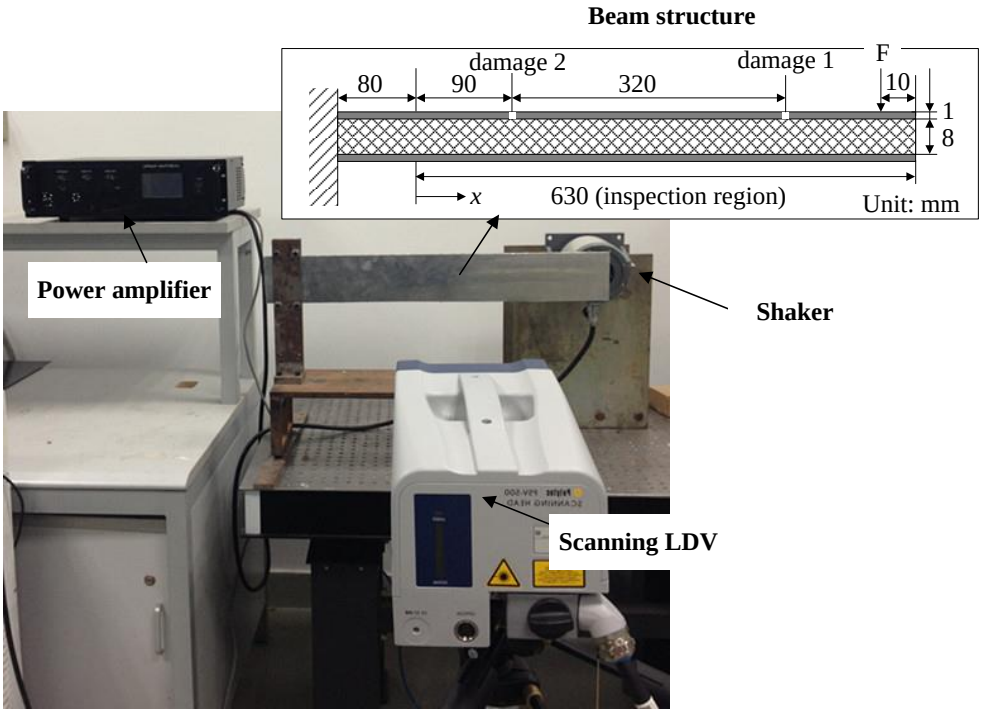

Fig. 14. Experimental setup.

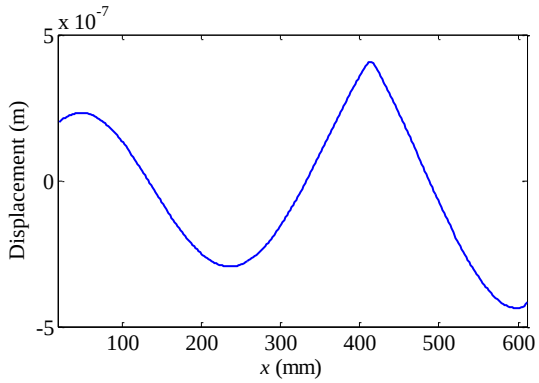

Fig. 15. Steady-state vibration displacement captured experimentally.

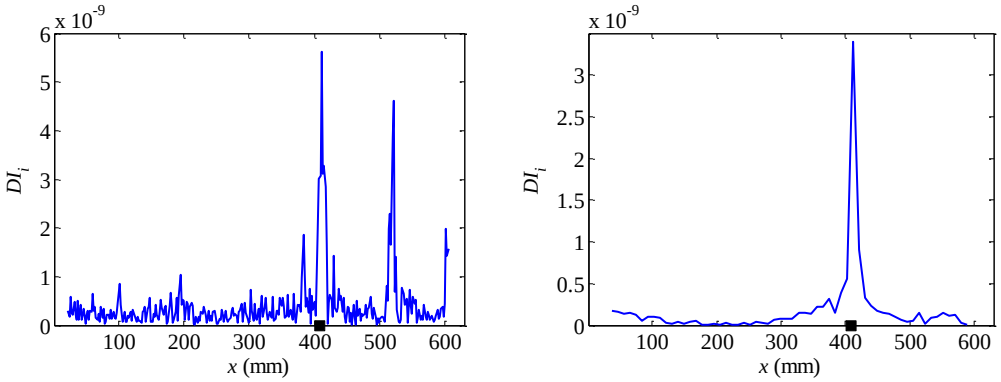

Fig. 16. Single damage detection results using DI_i with different intervals d:

(a) d=1.8 mm; (b) d=9.1 mm.

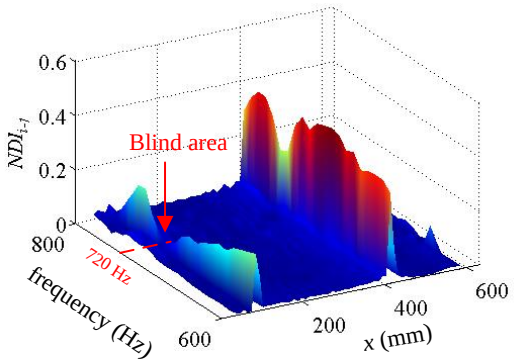

Fig. 17. Dual damage detection result using $NDI_{i\text{-}f}$.

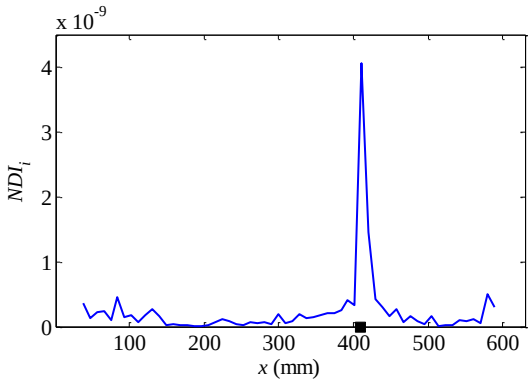

Fig. 18. Dual damage detection result using NDI_i at f=720 Hz.

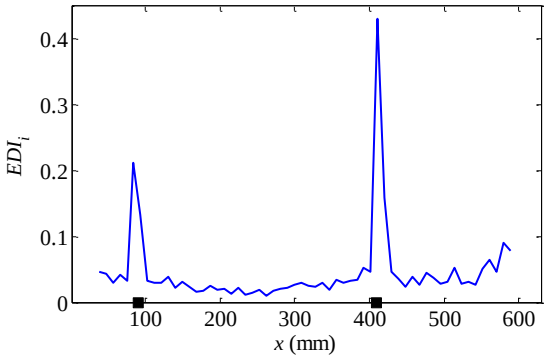

Fig. 19. Dual damage detection result using EDI_i.